Improved hydrogen storage properties of Mg/MgH2 thanks to the addition of nickel hydride complex precursors

Basile Galey, Aline Auroux, Sylviane Sabo-Etienne, Sameh Dhaher, Mary Grellier, Georgeta Postole

Improved hydrogen storage properties of Mg/MgH_2 thanks to the addition of nickel hydride complex precursors

Basile Galey[a], Aline Auroux[a], Sylviane Sabo-Etienne[b], Sameh Dhaher[b], Mary Grellier[b], Georgeta Postole[a]**

[a] *Univ Lyon, Université Claude Bernard Lyon 1, CNRS, IRCELYON, F-69626, Villeurbanne, France*
[b] *LCC-CNRS, Université de Toulouse, CNRS, UPS, 205 route de Narbonne, BP 44099, F-31077 Toulouse Cedex 4, France.*

Corresponding authors: georgeta.postole@ircelyon.univ-lyon1.fr
basile.galey@ircelyon.univ-lyon1.fr

Abstract

In order to improve the hydrogenation/dehydrogenation properties of the Mg/MgH_2 system, the nickel hydride complex $NiHCl(P(C_6H_{11})_3)_2$ has been added in different amounts to MgH_2 by planetary ball milling. The hydrogen storage properties of the formed composites were studied by different thermal analyses methods (temperature programmed desorption, calorimetric and pressure-composition-temperature analyses). The optimal amount of the nickel complex precursor was found to be of 20 wt%. It allows to homogeneously disperse 1.8 wt% of nickel active species at the surface of the Mg/MgH_2 particles. After the decomposition of the complex during MgH_2 dehydrogenation, the formed composite is stable upon cycling at low temperature. It can release hydrogen at 200 °C and absorb 6.3 wt% of H_2 at 100 °C in less than one hour. The significantly enhanced H_2 storage properties are due to the impact of the highly dispersed nickel on both the kinetics and thermodynamics of the Mg/MgH_2 system. The hydrogenation and dehydrogenation enthalpies were found to be of -65 and 63 kJ/mol H_2 respectively (± 75 kJ/mol H_2 for pure Mg/MgH_2) and the calculated apparent activation energies of the hydrogen uptake and release processes are of 22 and 127 kJ/mol H_2 respectively (88 and 176 kJ/mol H_2 for pure Mg/MgH_2). The change in the thermodynamics observed in the formed composite is likely to be due to the formation of a $Mg_{0.992}Ni_{0.008}$ phase during dehydrogenation/hydrogenation cycling. The impact of another hydride nickel precursor in which chloride has been replaced by a borohydride ligand, namely $NiH(BH_4)(P(C_6H_{11})_3)_2$, is also reported.

Keywords

Hydrogen storage, MgH_2, nickel hydride complex, thermodynamics, kinetics.

1. Introduction

Magnesium hydride, MgH_2, has been widely recognized as a promising solid-state hydrogen storage material due to its high volumetric (0.11 kg H_2/l) and gravimetric (7.65 wt% H_2) capacities [1]. However, the practical applications are so far limited by the high thermodynamic stability of the Mg/MgH_2 system ($\Delta H = \pm 75$ kJ/mol H_2), slow hydrogenation and dehydrogenation kinetics and poor cycle lifespan stability of nanostructured MgH_2 at high temperatures [2,3]. The advantages/limits of the Mg/MgH_2 storage system are compared in Table 1 with the ultimate technical targets given by the DOE (U.S. Department of Energy) for on-board hydrogen storage for light-duty vehicles [4,5].

Table 1 – Technical targets given by the DOE for onboard hydrogen storage for light-duty vehicles

Storage parameters	2020	2025	Ultimate	Mg/MgH_2
System gravimetric capacity (wt % H_2)	4.5	5.5	6.5	7.65
System volumetric capacity (kg H_2/l)	0.03	0.04	0.05	0.11
Min/max delivery temperature (°C)	-40/85	-40/85	-40/85	350-400
Operational cycle life (cycles)	1500	1500	1500	>1500
System fill time (min)	3-5	3-5	3-5	too slow
Fuel cost ($/kg H_2)	333	300	266	cheap

Magnesium hydrogenation is an exothermic reaction. The hydrogen uptake mechanism, already reported in the literature, is well described by Bérudé et al. [6]. Hydrogenation of bulk magnesium is kinetically unfavourable at ambient temperature due to the slow diffusion process of H in Mg, the presence of an $MgO – Mg(OH)_2$ oxide layer covering the surface of magnesium particles and the large energy necessary to split H_2 molecules at the magnesium surface [7]. Hydrogenation kinetics can be significantly improved by ball milling preparation and proper catalyst addition [8]. The nanostructuration allows to minimize the diffusion issue and to partially break the oxide layer [9] while doping with transition metal nanoparticles or oxides provides sites for dissociative adsorption of H_2 [6,10]. Chen et al. [11] reported a composite able to store 5.2 wt% of H_2 in less than 5 minutes at 80 °C thanks to the addition of ZrO_2 to MgH_2 with a molar ratio of 5:95. Chen et al. [12] doped MgH_2 with a Ni/TiO_2 nanocomposite allowing the system to absorb 5.3 wt% of H_2 in 7 min at 100 °C. Many other systems able to absorb around 5wt% of hydrogen at temperatures lower than 100 °C have been reported but they are most of the time limited by their dehydrogenation properties [11–16].

Dehydrogenation of magnesium hydride is an endothermic reaction which is thermodynamically unfavourable at low temperatures [17]. For pristine MgH_2, temperatures higher than 400 °C are required for hydrogen release with a dehydrogenation enthalpy and entropy of 74.7 kJ/mol H_2 and 130 J/K.mol H_2, respectively [18,19]. Hydrogen desorption kinetics are also very low and the mechanisms for the dehydrogenation reaction are reverse from the hydrogenation of Mg [20]. Nanostructuration of MgH_2 and transition metal nanoparticles or oxide addition significantly enhance the dehydrogenation kinetics allowing hydrogen release temperatures as low as 200 °C [15,21–25]. For example, the systems

formed by Chen et al. [11] and Chen et al. [12] are able to desorb 6.0 wt% of H_2 at 240 °C in 50 min and 4.5 wt% of H_2 at 210 °C in 100 min, respectively. Kumar et al. [21] added 5 wt% of nanometric iron to MgH_2 by planetary ball milling and prepared a composite which releases 6.5 wt% of H_2 in between 175 and 250 °C. Zhang et al. [22] used lithium metatitanate to dope MgH_2 allowing a decomposition temperature as low as 211 °C. However, these systems are most of the time limited by the high thermodynamic stability of Mg/MgH_2, and, in order to further reduce the dehydrogenation temperature, the Mg-H bond needs to be destabilized. Shinde et al. [26] designed a system able to release H_2 at temperatures lower than 150 °C by embedding MgH_2 nanoparticles in 3-D activated carbon with periodic synchronization of nickel. Indeed, the authors succeeded to significantly enhance the dehydrogenation kinetics and thermodynamics of MgH_2 and to decrease both the apparent activation energy and reaction enthalpy from 160 to 43 kJ/mol and from 74.7 to 49.1 kJ/mol H_2, respectively. However, although not mentioned in the reported study, with a MgH_2 loading of 60 wt% in the carbon structure, the overall hydrogen storage capacity of the system should decrease in consequence. Thus, up to now, no systems with dehydrogenation properties within the ultimate DOE targets have been reported yet and further research work is needed.

Among the different catalysts studied, nickel has been recognized as one of the most efficient thanks to a low cost and a significant impact on both hydrogenation and dehydrogenation [12,14,15,26,27]. The catalytic activity of Ni is mainly attributed to its high affinity toward H, which helps to destabilize the Mg-H bond and facilitate its dissociation [8]. Nickel also provides sites for dissociative adsorption of H_2, subsequent migration of hydrogen atoms onto adjacent Mg surface via spillover and further surface diffusion [10]. According to Dai et al. [28], during dehydrogenation, nickel can attract H atoms to form a Mg_2NiH_4 phase thermodynamically less stable than MgH_2, impacting the overall dehydrogenation thermodynamics. The catalytic activity of nickel is highly dependent on the site density of the Ni active sites over MgH_2 surface as highlighted by Yang et al. [29]. The authors [29] suggested that nanostructured MgH_2 could desorb hydrogen from 100 °C, if the number of catalyst sites was around 4×10^{14} per m^2 of MgH_2. To achieve such a goal, a control of the size of the nickel species used to dope MgH_2 is mandatory. Nanoscale or cluster-scale nickel additives allow more sites to interact with MgH_2 surface and therefore to be active. In previous works, our group [30,31] and Kumar et al. [14,16] studied the impact of the addition of transition metal complexes on the hydrogen storage properties of the Mg/MgH_2 system. The results demonstrated that the complexes play the role of precursors and allow a homogeneous dispersion of atomic or cluster-scale active species at the surface of MgH_2. High hydrogenation and dehydrogenation kinetics were obtained in comparison with pure milled MgH_2. However, either the lifespan stability of the formed composite was not addressed [14,16] or it was poor [30,31] due to the nature of the metal centers involved. In our previous work [31], we have shown that only the addition of a high amount of nickel and iron nanoparticles, 10 and 5 wt% respectively, to a "MgH_2 + complex" system allowed to preserve upon cycling the positive impact of the complex on the hydrogenation/ dehydrogenation properties.

The present study follows these previous works [14,16,30,31] and shows the impact of a well-defined nickel hydride complex, $NiHCl(P(C_6H_{11})_3)_2$ labelled NiHCl throughout the paper, on the hydrogen storage properties of the Mg/MgH_2 system. Different amounts of the complex were added to MgH_2 by planetary ball milling in order to find the optimal site density of the Ni active sites and the corresponding "MgH_2 - NiHCl" mixtures were characterized by various techniques. The hydrogen storage properties of the formed composites have been studied with a particular attention to the cycle lifespan stability. Moreover, the chloride present in the NiHCl complex was substituted by a borohydride ligand and the corresponding nickel borohydride precursor $NiH(BH_4)(P(C_6H_{11})_3)_2$, labelled $NiH(BH_4)$, was also tested as an additive to MgH_2.

2. Experimental

2.1. Materials

The magnesium hydride powder was provided by McPhy Company (La Motte-Fanjas, France) and its physico-chemical and hydrogen storage properties were reported elsewhere [30,31]. XRD patterns revealed the presence of low amounts of Mg and MgO (5 and 4 wt%, respectively, as evaluated from Rietveld refinement) in as-received MgH_2. The hydrogen storage capacity of the Mg/MgH_2 system was measured to be of 7.0 wt%, as expected given the powder purity. The nickel hydride complexes, $NiHCl(P(C_6H_{11})_3)_2$, namely here NiHCl, and $NiH(BH_4)(P(C_6H_{11})_3)_2$, labelled $NiH(BH_4)$, were synthesized based on procedures previously reported [32-34]. Fig. 1 shows their schematic representations (PCy_3 = $P(C_6H_{11})_3$). The complexes were characterized by ^1H, ^{13}C and ^{31}P solution and solid state NMR experiments as presented in Fig. S1 and S2.

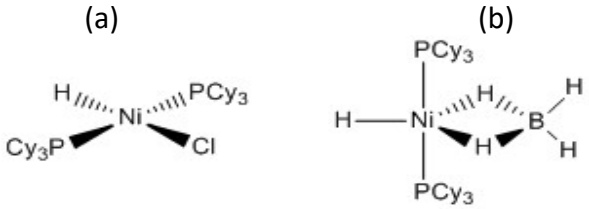

Fig. 1 – Schematic representation of the nickel hydride complexes used in the study (a) $NiHCl(P(C_6H_{11})_3)_2$ and (b) $NiH(BH_4)(P(C_6H_{11})_3)_2$.

All the mixtures of MgH_2 with different amounts of the nickel hydride precursor were prepared by planetary ball milling using a PM100 apparatus from Retsch under an inert argon atmosphere. The milling bowl was hermetically closed inside the glovebox to prevent any oxidation of the powders. The MgH_2 based storage systems were obtained by milling for 5 h using balls of zirconium dioxide of 1 mm diameter and a milling frequency of 300 revolutions per minute. The ball to powder mass ratio was 100:1. The rotation of the ball in the mill was paused every 2 min and inverted every 5 min to limit the temperature increase in the milling cell. Different amounts of NiHCl and $NiH(BH_4)$ complexes were added before milling to the commercial MgH_2 powder. The obtained composites were labelled in relation

with the complex used and its amount as follows: 5-NiHCl, 10-NiHCl, 20-NiHCl, 25-NiHCl and 50-NiHCl for MgH_2 milled with 5, 10, 20, 25 and 50 wt% of NiHCl, respectively, and 5-$NiHBH_4$, 10-$NiHBH_4$ and 20-$NiHBH_4$ for the mixtures "MgH_2 + $NiH(BH_4)$". For comparison, MgH_2 was grinded under the same conditions without any additive and the obtained powder is denoted as 100-MgH_2. Table 2 shows the different MgH_2-based mixtures studied in this work and the labels used further on. The nickel content in the formed composite is also reported in the table.

Table 2: Studied MgH_2-based storage systems: label and composition

System label	NiHCl (wt%)	$NiH(BH_4)$ (wt%)	MgH_2 (wt%)	Ni content (wt%)
100-MgH_2	0	0	100	0
5-NiHCl	5	0	95	0.45
10-NiHCl	10	0	90	0.89
20-NiHCl	20	0	80	1.79
25-NiHCl	25	0	75	2.24
50-NiHCl	50	0	50	4.47
5-$NiHBH_4$	0	5	95	0.46
10-$NiHBH_4$	0	10	90	0.92
20-$NiHBH_4$	0	20	80	1.85

2.2. Characterization

The X-Ray Diffraction (XRD) structural characterization of the samples was carried out with a Bruker D8 Advance A25-ray diffractometer using Cu–Kα radiation. The diffraction patterns were analysed by the Rietveld method, using the Topas software to determine the crystallites mean size. X-ray sample holders were filled inside the glove box and covered with a kapton foil to minimize air contact during X-ray measurements.

The surface morphology of the formed composites was investigated with a FEI TITAN ETEM G2 80–300 kV instrument (0.085 nm resolution) equipped with an objective Cs aberration corrector. The microscope was also equipped with an energy dispersive X-ray (EDX) analyser (SDD X-Max 80 m m^2 from Oxford Instruments). The samples were crushed in ethanol and the solution was ultrasonically stirred before dropping it on a holey carbon-covered copper TEM grid, followed by drying.

2.3. Storage properties

The temperature stability of the complexes was analysed by Thermogravimetric Analysis (TGA) with a TG Discovery from TA Instruments. The analyses were performed from ambient to 450 °C (heating rate of 2 °C/min) under an argon flow of 25 mL/min. Hermetic aluminium pans with a pin hole, sealed inside the glove box, were used to prevent any oxidation.

The dehydrogenation properties of the different storage systems were studied by Temperature Programmed Desorption (TPD) with a TPD/R/O-1100 apparatus from Thermo. The analyses were performed from ambient temperature to 450 °C (2 °C/min) under an argon flow of 40 mL/min. A calibration curve obtained from the reduction of different

masses of copper (II) oxide was used to determine the amount of hydrogen desorbed by the samples. The TPD instrument is coupled with a mass spectrometer OmniStar^{TM} from Pfeiffer Vacuum, allowing to study the nature of the decomposition gazes.

Calorimetric measurements were performed with a DSC Q100 from TA Instruments by using hermetic aluminium pans with a pin hole, sealed inside the glovebox. The measurements were carried out under a flow of high-purity argon (40 mL/min) at different heating rates (2, 5, 7.5 and 10 °C/min) from room temperature to 450 °C. The apparent activation energy of the dehydrogenation process was determined using Kissinger's method as described elsewhere [30,35,36].

The thermodynamic properties of the samples were determined by making Pressure-Composition-Temperature (PCT) analyses with a HVPA-200 Sievert's apparatus from Micromeritics. Before the PCT experiments, the powders obtained just after milling were degassed under vacuum at 300 °C. The hydrogenation/ dehydrogenation isotherms were performed at 300, 325 and 350 °C. Formation enthalpies and entropies of both hydrogenation and dehydrogenation were calculated using Van't Hoff method [6,30,37,38].

The HVPA-200 Sievert's apparatus was also used to study the hydrogenation kinetics of the composites. Hydrogen absorption isotherms were performed at various temperatures (50, 75, 100, 150, 200, 300, 325 and 350 °C) under 30 bar of H_2. Before the isotherms, the powders were degassed under vacuum at temperatures between 200 and 300 °C (the lowest temperature possible based on the TPD data to ensure the complete dehydrogenation of the sample). The apparent activation energy of the hydrogenation process was determined using the Johnson-Mehl-Avrami-Kolmogorov model as described in the ESI (eqns. S1 and S2) [11,13,15,39].

Finally, in order to study the reversibility of the formed storage systems, dehydrogenation/ hydrogenation cycles were performed under the following temperature and pressure conditions: dehydrogenation under vacuum at 200 °C and hydrogenation under 30 bars of H_2 at 100 °C. The evolution of the hydrogen release properties of the different storage systems was monitored by performing TPD analyses from ambient temperature to 450 °C (2 °C/min) under argon flow (40 mL/min) after each dehydrogenation/hydrogenation cycle. The results obtained were compared with dehydrogenation properties of the freshly prepared composites (just after milling).

3. Results and discussion

3.1. Thermal stability of NiHCl complex

With the aim to improve the properties of the hydrogen storage system, NiHCl complex was chosen as an additive to Mg/MgH_2 based on our previous study [31] using bis-(tricyclohexylphosphine)nickel(II) dichloride [$NiCl_2(P(C_6H_{11})_3)_2$]. In this previous work [31], we reported on the impact of such a complex on the homogeneous dispersion of nickel at the surface of MgH_2 particles during milling preparation. The results showed that the presence of two chlorine atoms allowed a positive effect on the thermal stability of the complex but presented a negative impact on the decomposition kinetics of MgH_2, therefore limiting the

amount of nickel that could be added to the Mg/MgH_2 system. Consequently, finding a good balance in between the thermal stability of the complex provided by chlorine and the amount of nickel to be added to the storage system was necessary. With that in mind, NiHCl complex has been chosen for the present study. It is composed with the same tricyclohexylphosphine ligands ($P(C_6H_{11})_3$ or PCy_3) as in the previously used complex, the same transition metal, nickel, but contains only one chloride instead of two.

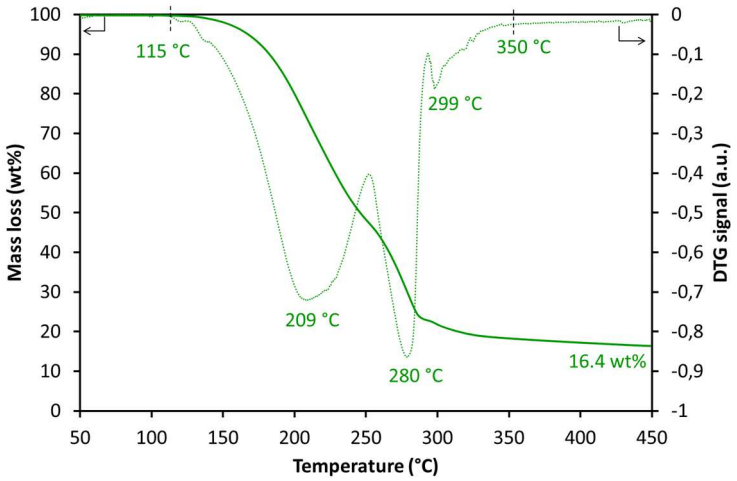

Fig. 2 – Thermogravimetric analyses of NiHCl complex heated under argon to 450 °C (2 °C/min): mass loss and DTG signal.

Fig. 2 presents the thermogravimetric analysis of the nickel hydride complex NiHCl. Mass loss and DTG signals are presented as a function of temperature. The decomposition starts around 115 °C, reaches its maximum rate at 209 °C, and is complete at 350 °C. At 450 °C, the complex is decomposed at 83.6 wt%, the remaining 16.4 wt% corresponding to the mass of the Ni and Cl atoms presents in $NiHCl(PCy_3)_2$ (theoretical value of 14.3 wt%). Therefore, with the NiHCl complex, after complete decomposition of the organic ligands, the amount of chlorine remaining is half than in the case of $NiCl_2(PCy_3)_2$, for the same amount of nickel dispersed.

3.2. Optimization of the amount of NiHCl complex

The dehydrogenation properties of the "MgH_2 - NiHCl" composites with different amounts of complex (5, 10, 15, 20, 25 and 50 wt%) and of pure milled MgH_2 were investigated by temperature programmed desorption (TPD), in order to design the system with the best H_2 release temperature/H_2 storage capacity. Fig. 3 presents the temperature profiles of MgH_2 decomposition (a) and the hydrogen capacity (b) of the "MgH_2 - NiHCl" composites, in comparison with 100-MgH_2. In Table 3, the onset and dehydrogenation peak maximum temperatures as well as the amount of hydrogen released are summarized.

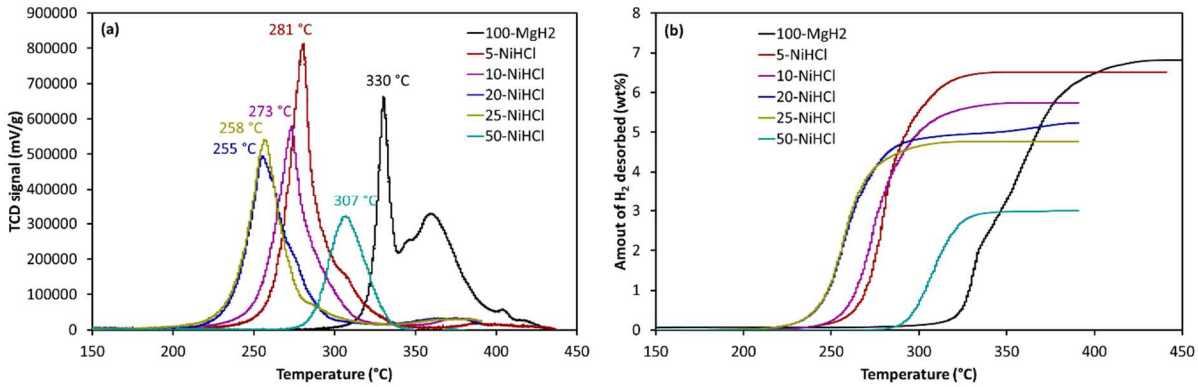

Fig. 3 – (a) TPD profiles and (b) corresponding thermally programmed H_2 desorption capacities curves of studied MgH_2-based powders. Experiments performed under argon from 40 to 450 °C with a heating rate of 2 °C/min.

Table 3 – Dehydrogenation properties of the storage systems: TPD results				
Samples	Onset temperature (°C)	Peak temperature (°C)	Hydrogen released [a] (wt%)	Normalized hydrogen released [b] (wt%)
100-MgH_2	310	330 – 360	6.8	7.5
5-NiHCl	240	281	6.5	7.7
10-NiHCl	223	273	5.7	7.2
20-NiHCl	199	255	5.2	7.5
25-NiHCl	195	258	4.8	7.3
50-NiHCl	265	307	3.0	7.5

[a] g_{H_2}/g_{sample}
[b] g_{H_2}/g_{MgH_2}

100-MgH_2 sample desorbs 6.8 wt% of hydrogen within a broad temperature range (300 to 400 °C) which is due to a large MgH_2 particles size distribution [30,31]. In comparison with pure-milled MgH_2, all the "MgH_2 - NiHCl" composites exhibit improved dehydrogenation properties. The onset hydrogen released temperatures are up to 115 °C lower than that of 100-MgH_2 and the TPD peaks are narrower (Fig. 3a) thanks to the positive impact of the complex on the limitation of the powder aggregation during milling preparation as previously reported [30,31]. The amount of hydrogen released varies between 6.5 and 3.0 wt% depending on the quantity of added complex.

Among all the presented systems, 20-NiHCl composite shows the best hydrogen release properties, with an onset dehydrogenation temperature lower than 200 °C, a maximum of decomposition at 255 °C and more than 5 wt% of H_2 desorbed before 300 °C. The obtained TPD peak temperature is almost 20 °C lower than the best composites using transition metal complexes reported in [31] and [14] (decomposition at 272 °C for "MgH_2 + 5 wt% of $NiCl_2(PCy_3)_2$" and 275 °C for "MgH_2 + 10 wt% $Ni(C_5H_5)_2$"), 30 °C lower than the one reported in [30] (MgH_2 + 10 wt% of $RuH_2(H_2)_2(PCy_3)_2$) and in the same temperature range as in Kumar et al. [16] (decomposition at 250 °C for "MgH_2 + 10 wt% $V(C_5H_5)_2$").

By comparing 20-NiHCl performances with the results obtained for 10-NiHCl and 5-NiHCl composites it can be observed that the dehydrogenation temperature peaks are shifted towards higher values by 18 and 26 °C, respectively. On the other hand, the H_2 storage capacity of 20-NiHCl is lower in comparison with 5-NiHCl and 10-NiHCl (5.2 against 5.7 and 6.5 wt% respectively, Table 3) due to the lower amount of MgH_2 and consequently of hydrogen present in the composite (Table 2). In our former studies [30,31] we have shown that free-tricyclohexylphosphines (PCy_3, Cy = C_6H_{11}) present a catalytic effect on the MgH_2 dehydrogenation thanks to phosphorous active species *in-situ* formed during milling. However, increasing the amount of added PCy_3 from 5 to 20 wt% did not enhance significantly the H_2 desorption behaviour (5 wt% being sufficient to cover MgH_2 surface). The improved dehydrogenation properties when the amount of $NiHCl(PCy_3)_2$ complex increases up to 20 wt% is therefore not directly linked with the increase in the amount of the PCy_3 ligands. The main difference is in the nickel loading. 1.79 wt% of Ni is involved in 20-NiHCl against 0.89 and 0.45 wt% for 10-NiHCl and 5-NiHCl, respectively. Increasing the amount of nickel therefore allows to lower the dehydrogenation temperature, as already widely reported [15,29,41].

Interestingly, in our previous work [31], when $NiCl_2(PCy_3)_2$ complex was added as doping agent to MgH_2, the best results were obtained with the addition of only 5 wt% of complex. Increasing the amount of $NiCl_2(PCy_3)_2$ up to 20 wt% in order to increase the nickel loading did not further enhance the MgH_2 dehydrogenation kinetics due to the negative impact of the increasing amount of chlorine present in the system [31,41–43]. By decreasing the loading of chlorine in the formed composites when NiHCl complex is used, a higher amount of nickel can therefore be dispersed on MgH_2 particles while keeping the chlorine level in the systems low enough to enable the enhancement of the H_2 release kinetics thanks to Ni.

For the amounts of NiHCl complex higher than 20 wt% (25-NiHCl and 50-NiHCl composites) the obtained TPD peaks are shifted towards higher temperatures (Fig. 3a). Although the differences of dehydrogenation temperature between 20-NiHCl and 25-NiHCl are not significant (only 3 °C, Table 3), the overall H_2 storage properties of 20-NiHCl composite are superior to the ones of 25-NiHCl, especially concerning the storage capacity (5.2 against 4.8 wt% H_2, Table 3). When MgH_2 is doped with 50 wt% of NiHCl complex (50-NiHCl), the dehydrogenation properties are further degraded. The hydrogen release occurs at 307 °C and the H_2 storage capacity is almost divided by 2 in comparison with 20-NiHCl composite. The degradation of dehydrogenation properties of MgH_2 in 50-NiHCl composite can be the result of two combined effects: (i) a too high amount of chlorine present in the composite and possibly (ii) a non-optimal Ni site density over the MgH_2 particles, as revealed in [29]. Indeed, Yang et al. [29] showed by studying the decomposition of MgH_2 mixed with Ni particles of different sizes and contents that the effectiveness of the catalyst depends on its distribution and site density over hydrogen storage particles.

The findings in this work therefore point out the importance, when using Ni based complexes containing chlorine, to reach an optimal ratio between the dispersed active Ni sites density (widely reported to improve MgH_2 decomposition [15,29,40]) and the chlorine level (reported to inhibit the dehydrogenation of MgH_2 [31,41-43]) rather than just a high

weight percentage of nickel. Under the studied conditions, 20 wt% of the Ni hydride complex is the maximum amount to be added to MgH_2 in order to obtain a storage system with low hydrogen desorption onset and peak temperatures and a hydrogen capacity that still satisfies the practical requirement.

3.3 Effect of the nickel borohydride precursor $NiH(BH_4)(PCy_3)_2$ on MgH_2 dehydrogenation

To overcome the kinetic inhibitor effect of chlorine for MgH_2 decomposition, a new complex was synthesized by replacing the chloride present in NiHCl by a borohydride ligand. The obtained $NiH(BH_4)(PCy_3)_2$ complex was further tested as precursor of nickel for a homogeneous doping over the MgH_2 surface. The thermal stability of the complex was studied by thermogravimetric analysis while TPD technique was employed to follow the desorption characteristics of MgH_2 mixed with 5, 10, and 20 wt% of $NiH(BH_4)(PCy_3)_2$.

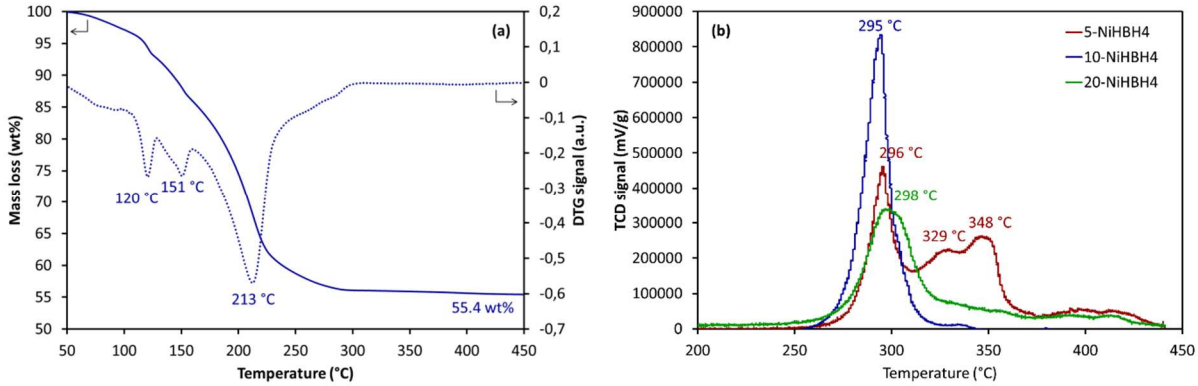

Fig. 4 – (a) Thermogravimetric analysis of $NiH(BH_4)(PCy_3)_2$ complex heated under argon to 450 °C (2 °C/min): mass loss and DTG signal. (b) TPD profiles of the studied "MgH_2 + $NiH(BH_4)(PCy_3)_2$" composites.

Fig. 4a presents the thermal decomposition of the $NiH(BH_4)(PCy_3)_2$ complex while the temperature profiles of hydrogen desorption (TPD plots) of the $NiHBH_4$ composites (5-$NiHBH_4$, 10-$NiHBH_4$ and 20-$NiHBH_4$) are shown in Fig. 4b. The decomposition of the complex starts around 50 °C, reaches its maximum rate at 213 °C and is completed at 300 °C. At 450 °C, the complex is decomposed at 44.6 wt%. Interestingly, the mass loss of a single PCy_3 ligand corresponds to a decrease in mass of 44 wt%. Although it is difficult to unambiguously give the structure of the remaining species, it is likely that the organic part of $NiH(BH_4)(PCy_3)_2$ is not fully decomposed at 450 °C, contrary with what is observed for NiHCl complex (Fig. 2).

The different thermal stability of $NiH(BH_4)(PCy_3)_2$ in comparison with $NiHCl(PCy_3)_2$ seems to impact the hydrogen storage properties of magnesium hydride as it can be seen in Figs. 4b and 3. The TPD profiles of the $NiHBH_4$ composites show that 10 wt% of $NiH(BH_4)(PCy_3)_2$ complex is the optimal amount to add to MgH_2. The formed system starts to release hydrogen at 260 °C with the peak temperature at 295 °C. The use of higher amount of

$NiH(BH_4)(PCy_3)_2$ complex does not yield additional improvement in the desorption temperature while reducing significantly the hydrogen storage capacity (4.5 wt% for 20-$NiHBH_4$ against 6.2 wt% for 10-$NiHBH_4$). Concerning 5-$NiHBH_4$, the low amount of complex used seems to catalyse only partly the MgH_2 decomposition as confirmed by the presence of additional TPD peaks at 329 and 348 °C (in the temperature range of pure-milled MgH_2 dehydrogenation, Fig. 3a).

In comparison with the dehydrogenation properties of 20-NiHCl composite (hydrogen release at 255 °C, Fig. 3a), the hydrogen desorption temperatures are significantly higher when $NiH(BH_4)(PCy_3)_2$ complex is used. This behaviour may be related with the *in situ* formed species on the MgH_2 surface by the partial decomposition of $NiH(BH_4)(PCy_3)_2$ complex which may present a lower catalytic effect than the highly dispersed nickel (Fig. 4a). The use of such a thermally stable species may restrict the direct contact of Ni atoms with MgH_2 particles. On the contrary, for "MgH_2 – NiHCl" composites, the two PCy_3 ligands decompose before 300 °C (Fig. 2) allowing the dispersed nickel to interact with MgH_2 and enhance the dehydrogenation kinetics. Therefore, the substitution of chloride in NiHCl by a borohydride ligand does not allow to further improve the hydrogen storage properties of "MgH_2 – complex" based composites. These results open new perspectives concerning the use of such complexes as precursors of nickel catalyst for improving the hydrogen released of MgH_2. When replacing the chlorine by another element or ligand, parameters such as the thermal stability of the new formed complex and the kinetic impact on MgH_2 decomposition of the *in situ* formed species by the complex degradation during milling and/or first dehydrogenation step may be considered.

3.4 Hydrogenation/dehydrogenation cycle lifespan behaviour of 20-NiHCl composite

Among all the formed "MgH_2 - complex" composites, it was found that 20-NiHCl sample possesses the best dehydrogenation properties. Therefore, only its hydrogen storage properties were further explored through dehydrogenation/hydrogenation cycling. Although not systematically addressed in the studies using transition metal complexes as doping agent to Mg/MgH_2 [14,16], the degradation of the storage performances due to particles sintering during cycling is one of the major limitations of the use of nanostructured systems [2,6,17,31,44]. Changes in the hydrogen storage behaviour of 20-NiHCl composite are therefore expected after cycling, especially taking into account the thermal stability of the Ni-complex (Fig. 2) whose organic part may decompose during the first dehydrogenation step after grinding preparation.

In order to confirm this hypothesis, a TPD experiment was performed for 20-NiHCl just after milling and the released species in the gas phase were continuously monitored by MS. Signals corresponding to H_2 (m/z=2) and various carbon structures (e.g. cyclohexyl and benzene at m/z = 83 and 78, respectively) arising from complex degradation have been observed and are displayed in Fig. S3. The organic part of NiHCl complex (PCy_3 ligands) is therefore not preserved after the composite's first dehydrogenation. Based on these results, it is likely that the first dehydrogenation step induces two changes to the system: (i) the homogeneous dispersion of nickel active sites over Mg/MgH_2 particles (expected to have a

beneficial impact on the storage properties) (ii) the decomposition of the PCy_3 ligands and so of the active phosphorus based species formed *in-situ* during milling and presenting a significant positive impact on the hydrogen release kinetics [30,31].

Fig 5a presents the TPD curves obtained for 20-NiHCl after dehydrogenation/hydrogenation cycling under different conditions: (i) low temperature (dehydrogenation and hydrogenation at 200 and 100 °C respectively) and (ii) high temperature (after 3 PCT experiments performed at 300, 325 and 350 °C). The evolution of the amount of hydrogen released as a function of temperature is given in Fig. 5b. The results obtained for the fresh-milled powder is also shown for comparison. In Fig 5c are presented the corresponding hydrogenation isotherms performed under 30 bars of H_2 at 100 °C.

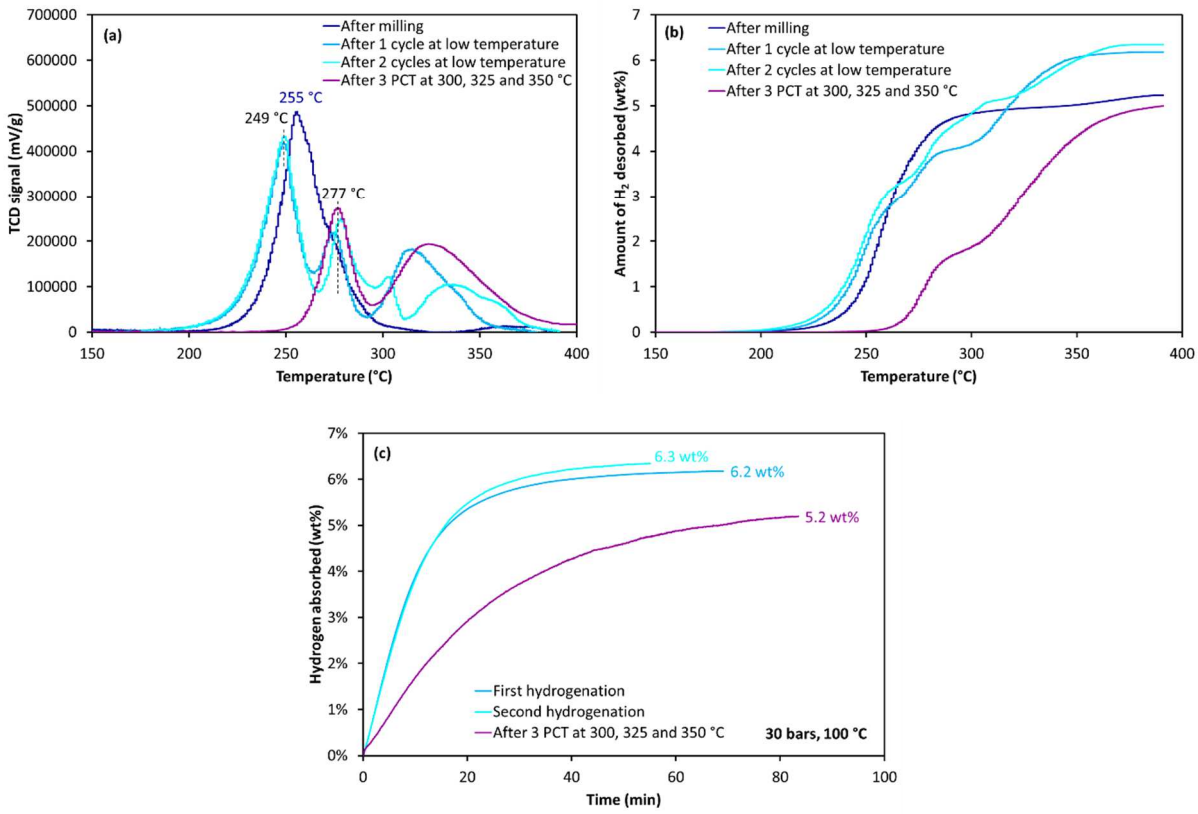

Fig. 5 – (a) TPD profiles, (b) corresponding thermally programmed H_2 desorption capacities curves and (c) the isothermal rates of hydrogenation at 100 °C under 30 bars H_2. Comparison of 20-NiHCl just after milling and after hydrogenation/dehydrogenation cycles under different temperatures.

The TPD curves presented in Fig. 5a show, indeed, changes in the dehydrogenation properties of MgH_2 after the decomposition of the NiHCl complex organic part (PCy_3 ligands). 20-NiHCl after one dehydrogenation/hydrogenation cycle, performed at low temperature, starts to release hydrogen at 180 °C and allows to desorb 6.2 wt% of H_2, an amount almost 20 % higher than the H_2 content in the freshly prepared composite (5.2 wt% H_2 in 20-NiHCl just after milling, Fig. 5b). The decomposition profile splits into three maxima with a main peak at 249 °C and two other peaks at 277 and 314 °C. After two hydrogen

adsorption/desorption cycles at low temperature, similar dehydrogenation properties are observed, with an onset temperature slightly lower at 175 °C, a maximum dehydrogenation rate reached at 249 °C and 3 less intense peaks at 277, 303 and 333 °C. The amount of hydrogen released is of 6.3 wt%. When 20-NiHCl is investigated after 3 PCT experiments at 300, 325 and 350 °C, the TPD profile shows degraded hydrogen released properties. The H_2 storage capacity is decreased to 5.2 wt%, the onset dehydrogenation temperature shifts to higher values (235 °C) and the decomposition curve presents two maxima at 277 and 325 °C. It is interesting to note that the dehydrogenation peak around 277 °C is common to all the decomposition profiles (a small shoulder is visible at 277 °C for fresh-milled 20-NiHCl composite, Fig. 5a).

Fig. 5c presents the hydrogenation isotherms at 100 °C of 20-NiHCl composite under the different cycling conditions. No significant differences are noticeable between the first and the second hydrogenation of 20-NiHCl under low temperature conditions. The composite is thus able to absorb around 6.0 wt% of H_2 at 100 °C in less than 30 min irrespective of the number of cycles. The hydrogenation kinetics of 20-NiHCl after 3 PCT at high temperature are significantly decreased and the composite is only able to absorb 5.0 wt% of H_2 in more than 1 hour.

Comparing these performances with those previously reported by our group [30,31], 20-NiHCl is the first transition metal complex – MgH_2 composite that improves and further preserves its dehydrogenation properties during cycling at low temperature. The hydrogenation rates at 100 °C are also significantly higher than the one reported in [30,31]. This is most likely thanks to the higher amount of nickel (1.79 wt%) doping the Mg/MgH_2 surface after the decomposition of the organic part of the complex during the first dehydrogenation. Based on these results, the behaviour of 50-NiHCl sample after cycling was also studied and is shown in Fig. S4. This composite, containing a much higher amount of nickel (4.48 wt%), does not present enhanced dehydrogenation properties after cycling (desorption of 4.1 wt% of H_2 at 329 °C) as observed for 20-NiHCl. The amount of nickel is therefore not the only parameter inducing the hydrogen storage properties enhancement of the Mg/MgH_2 system. It is more likely the site density of the catalyst over the MgH_2 particles surface that matters [29], and, the addition of around 1.8 wt% of Ni seems to allow reaching the optimal site density in this specific system and preparation conditions. Furthermore 2.5 time less chlorine is present in 20-NiHCl than in 50-NiHCl composite.

3.5 Dehydrogenation thermodynamics and kinetics of 20-NiHCl composite

To further study the hydrogen storage properties of 20-NiHCl composite, DSC experiments at different heating rates were performed in order to determine both the dehydrogenation reaction enthalpy and apparent activation energy. Three samples were studied and compared: fresh-milled 20-NiHCl, 20-NiHCl after two cycles at low temperature and 20-NiHCl after 3 PCT at high temperature, Figs. 6a-c. The reaction enthalpies were determined by integrating the dehydrogenation DSC peaks and the results were converted into standard conditions for temperature and pressure. The apparent activation energies were calculated by using Kissinger method [30,35,36]. Fig. 6d shows the corresponding Kissinger plot.

Table 4 summarizes the dehydrogenation properties of 20-NiHCl composite under the different cycling conditions. The data obtained for pure-milled MgH_2 are also shown for comparison, although reported in a previous work [31]. The dehydrogenation kinetics are enhanced in presence of NiHCl complex and the apparent activation energy of the different 20-NiHCl composites are decreased by around 25 % compared to 100-MgH_2 sample. Interestingly, the lowest value is obtained for two times cycled 20-NiHCl at low temperature. It is consistent with the obtained dehydrogenation temperature, which is also the lowest for this sample (Table 4). Concerning fresh-milled 20-NiHCl and 20-NiHCl after 3 PCT at high temperature, no significant differences in the apparent activation energy of dehydrogenation values are noticeable.

The heat involved in the dehydrogenation of 20-NiHCl composite after 3 PCT experiments is of 72 ± 4 kJ/mol H_2, the same than pure milled MgH_2 sample. It is in good agreement with the theoretical value of 74.7 kJ/mol H_2 as reported by Bogdanovic et al. [19] for the Mg/MgH_2 system. The dehydrogenation enthalpies of 100-MgH_2 and 20-NiHCl composite after 3 PCT were also calculated with PCT experiments and Van't Hoff method as presented in Fig. S5 and [30], the results showing no differences between the two samples (ΔH = 82 ± 6 kJ/mol H_2). However, for 20-NiHCl composite just after milling and after 2 cycles at low temperature, dehydrogenation enthalpy values of 65 ± 5 and 63 ± 3 kJ/mol H_2 were found, respectively, showing an impact of the complex on the thermodynamic stability of MgH_2.

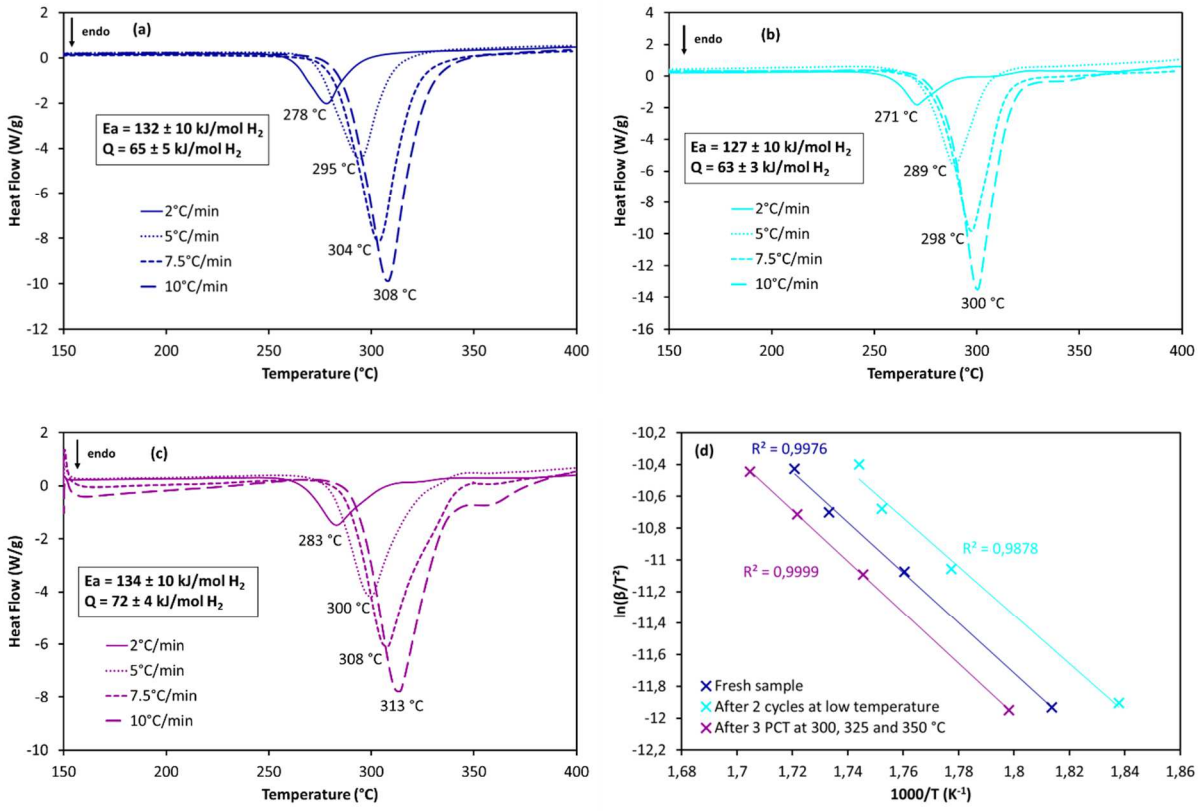

Fig. 6 – DSC curves at different heating rates of (a) fresh 20-NiHCl composite, (b) 20-NiHCl after 2 cycles at low temperature, (c) 20-NiHCl after 3 PCT experiments at high

temperature and (d) corresponding Kissinger plot. The DSC experiments were performed under argon at various heating rates: 2, 5, 7.5 and 10 °C/min.

Table 4 – Dehydrogenation properties of 20-NiHCl composite obtained by TPD and DSC

Samples	TPD			DSC	
	Onset T (°C)	Peak T (°C)	Storage capacity (wt%)	ΔH (kJ/mol H_2)	Ea (kJ/mol H_2)
100-MgH_2	310	330 – 360	6.8	72 ± 4	176 ± 14
Just after milling	199	255 – (277)	5.2	65 ± 5	132 ± 10
After 2 cycles	175	249 – 277 - 303	6.3	63 ± 3	127 ± 10
After 3 PCT	235	277 - 325	5.0	72 ± 4	134 ± 10

The addition of NiHCl complex to MgH_2 therefore leads to a change in both the dehydrogenation thermodynamics and kinetics in comparison with pure-milled MgH_2. The kinetics enhancement is maintained regardless of the dehydrogenation/hydrogenation cycling temperature conditions while the thermodynamic change is preserved only when the cycles are performed at low temperature (Table 4). The observed degraded dehydrogenation properties of 20-NiHCl after 3 PCT experiments in comparison with 20-NiHCl after 2 cycles at low temperature, Fig. 5a, is therefore due to the loss of the thermodynamic impact of NiHCl at high temperature. The change in the thermodynamic properties for 20-NiHCl composite is likely to be due to the presence of highly dispersed nickel at the surface of MgH_2 particles as reported by Xia et al. [45] and Shinde et al. [26]. Indeed, due to its high affinity toward H, Ni helps to destabilize the Mg-H bond and thus facilitates its dissociation [8].

Interestingly, the TPD curves obtained in Fig. 5a for 20-NiHCl presented different dehydrogenation profile. The first one around 250 °C is common to fresh-milled 20-NiHCl and 20-NiHCl after 2 cycles at low temperature and may therefore highlight the combinative kinetics and thermodynamics impacts of the highly dispersed nickel on the dehydrogenation properties of MgH_2. The second one at 277 °C is shared by all the samples and may illustrate the kinetics impact of the nickel individually. Finally, the TPD peaks obtained at temperatures higher than 300 °C for cycled composites may correspond to un-doped MgH_2. However, it is difficult to say either this behaviour comes from an inhomogeneous distribution of the nickel over MgH_2/Mg surface or from the fact that the nickel does not interact with the core of the MgH_2 particles.

3.6 Hydrogenation thermodynamics and kinetics of 20-NiHCl composite

To study in details the hydrogenation kinetics and thermodynamics of 20-NiHCl composite, the apparent activation energy and the hydrogenation enthalpy (and entropy) were determined using the Johnson-Mehl-Avrami-Kolmogorov (JMAK) model (eqns. S3 and S4) and Van't Hoff method (eqn. S2) respectively. Fig. 7a presents the hydrogenation isotherms performed under 30 bars of H_2 at 50, 75, 100, 150 and 200 °C for 20-NiHCl. The composite was dehydrogenated under vacuum at 200 °C before each isotherm. Fig. 7b shows the JMAK plot for the studied temperatures and Fig. 7c the corresponding Arrhenius plot. The

experiments performed for 100-MgH_2 are presented in Fig. S6. Finally, in Fig. 8a is shown the PCT hydrogenation isotherms while Fig. 8b presents the corresponding Van't Hoff plot, for 20-NiHCl composite.

As shown in Fig. 7a, 20-NiHCl composite is able to absorb 3 wt% of hydrogen in two hours at a temperature as low as 50 °C. At 200 °C, the composite can store 6 wt% of H_2 in less than 20 min. In comparison, more than 4 hours are required for pure-milled MgH_2 to absorb such an amount of H_2 at 200 °C (Fig. S6). The hydrogenation properties are therefore highly enhanced in presence of NiHCl, which is confirmed by the apparent activation energies calculated in Fig. 7c showing a drastic decrease for the Ea of 20-NiHCl in comparison with 100-MgH_2 (22 ± 6 against 88 ± 30 kJ/mol H_2). The impact of the dispersed nickel is thus significant on the hydrogenation kinetics of Mg. Indeed, Ni provides sites for dissociative adsorption of H_2, subsequent migration of hydrogen atoms onto adjacent Mg surface via spillover and further surface diffusion, as reported in the literature [7,8,10].

The hydrogenation PCT isotherms presented in Fig 8 allows to calculate the enthalpy and entropy of the reaction for 20-NiHCl composite. The results for 100-MgH_2 sample were already reported elsewhere [30], and the found enthalpy and entropy were -76 ± 2 kJ/mol H_2 and -138 ± 3 J/K.mol H_2 respectively (consistent with the theoretical values [19]). For 20-NiHCl composite, the values calculated by the Van't Hoff method are of -65 ± 4 kJ/mol H_2 and -120 ± 6 J/K.mol H_2 for the hydrogenation enthalpy and entropy, respectively. Thanks to NiHCl complex, the resulting dispersed nickel therefore impacts the hydrogenation thermodynamics of MgH_2 and that even at high temperatures (the PCT experiments were performed at 300, 325 and 350 °C).

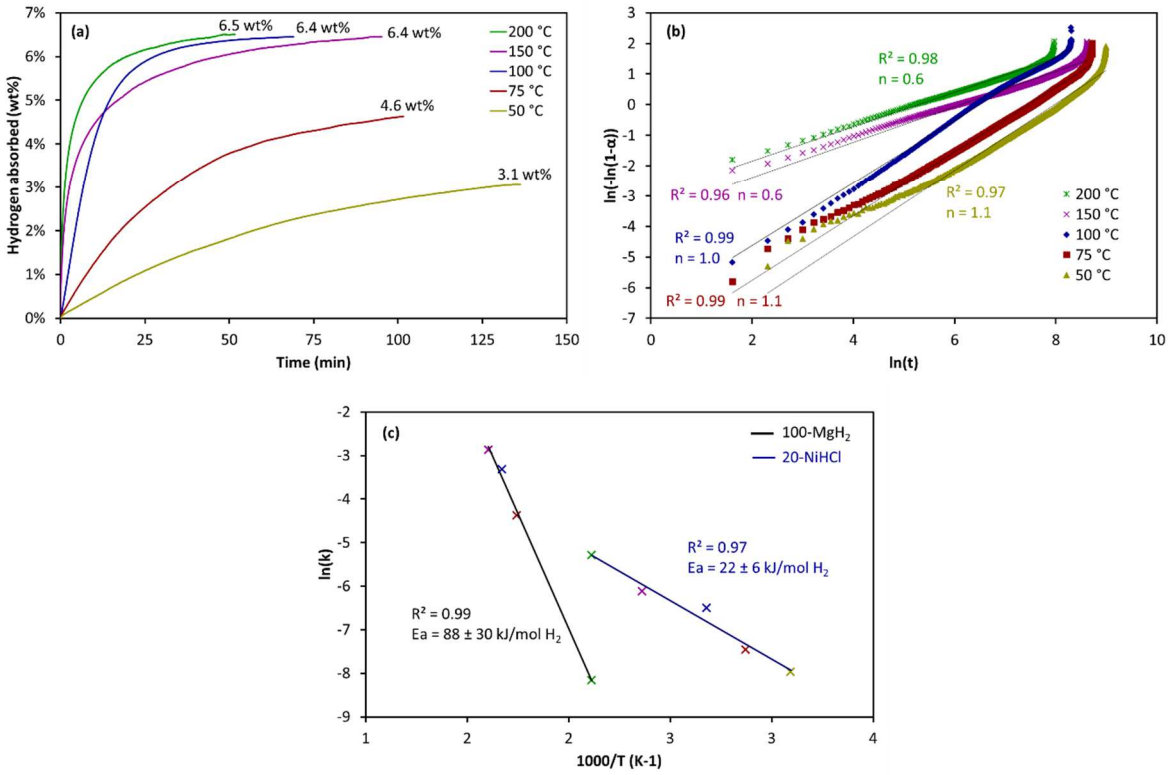

Fig. 7 – (a) Isothermal rates of hydrogenation under 30 bars H_2 at various temperatures, corresponding (b) JMAK plot and (c) Arrhenius plot for 20-NiHCl composite (and 100-MgH_2).

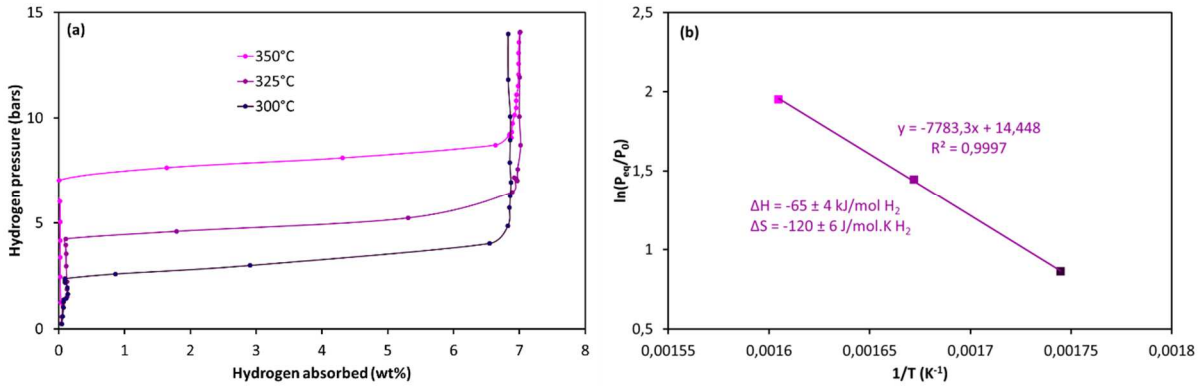

Fig. 8 – (a) hydrogenation PCT isotherms at high temperatures and (b) corresponding Van't Hoff plot for 20-NiHCl composite

3.7 Characterization and comparison with other hydrogen storage systems

To understand how NiHCl complex impacts the kinetics and thermodynamics of the Mg/MgH_2 system, 20-NiHCl composite was fully characterized by STEM, HRTEM/EDX, ^{13}C and ^{31}P NMR, XPS and XRD, under the different cycling conditions (just after milling, after 2 cycles at low temperature and/or after 3 PCT experiments). It is important to note that only the NMR and XRD experiments were performed under a controlled atmosphere allowing to prevent the oxidation of the composites. The NMR and XPS experiments are shown in Figs. S7 and S8 respectively. NMR provides confirmation of the decomposition of the organic part of the complex during the first dehydrogenation of 20-NiHCl composite. Indeed, the signals corresponding to phosphorous and carbon species are visible for the fresh-milled sample but not anymore after 1 dehydrogenation/hydrogenation cycle at low temperature. Furthermore, XPS confirms that only Ni and Cl atoms from the complex are remaining after 2 cycles as Ni 2p and Cl 2p signals are detected (Fig. S8b and S8c). However it is difficult to further exploit the results due to the uncontrolled preparation conditions (the samples were in contact with the air before the experiments, leading to important surface oxidation).

The elemental mapping of 20-NiHCl composite just after milling preparation and after 2 cycles at low temperature performed by HRTEM/EDX are presented in Fig. 9. The corresponding EDX element concentrations are summarized in Table S1 and the presence of a high amount of oxygen confirms the oxidation of the surface of MgH_2 particles due to the preparation conditions. Phosphorous is only visible for the fresh milled sample and chlorine as traces for both samples. Concerning nickel, the amount detected by EDX is in good agreement with the theoretical one (1.79 wt%) and the elemental mappings show that Ni is highly dispersed even after 2 cycles at low temperature. The HRTEM and STEM experiments

did not show the presence of Ni aggregates, even at very high resolution (0.085 nm). NiHCl precursor complex therefore allows to homogeneously disperse the nickel metal centre during milling preparation at an atomic or cluster scale. The hydrogenation/dehydrogenation cycling performed at low temperature allows to preserve this high dispersion, significantly enhancing the hydrogen storage properties of the Mg/MgH_2 system. However, as presented in Fig. S9, the STEM images of 20-NiHCl composite after 3 PCT at 300, 325 and 350 °C show the presence of nickel nanoparticles of a few nanometres size at the surface of MgH_2. The nickel dispersed at an atomic scale through the complex decomposition aggregates during hydrogenation/dehydrogenation cycles performed at high temperatures. This phenomenon was not observed when similar cycling was performed at low temperatures (hydrogenation at 100 °C and dehydrogenation at 200 °C). The changes induced by nickel aggregation in the active sites distribution at the surface of MgH_2 particles may explain the dehydrogenation properties degradation of 20-NiHCl composite after 3 PCT at 300, 325 and 350 °C (Fig. 5). Interestingly, the dehydrogenation enthalpy increases from 63 ± 3 to 72 ± 4 kJ/mol H_2 (similar to pure milled MgH_2, Table 4) showing changes in the thermodynamic properties after cycling at high temperatures.

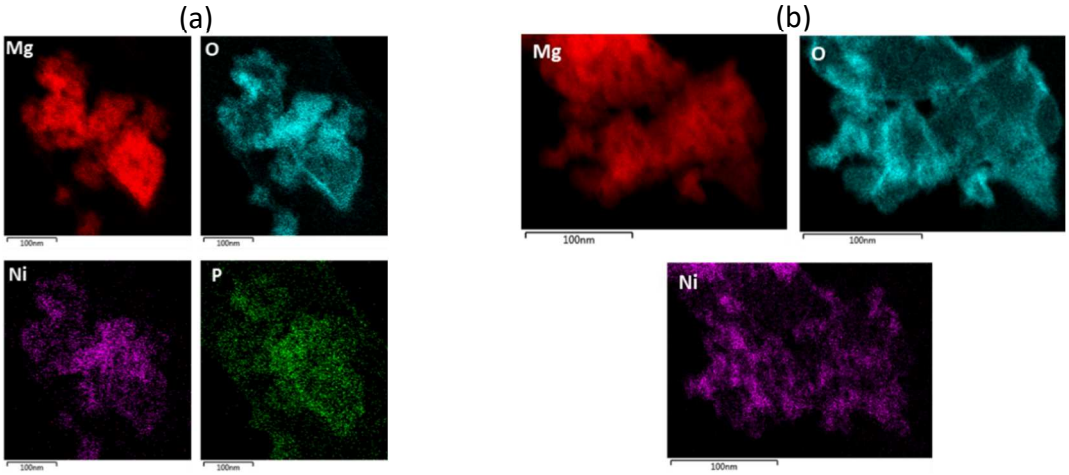

Fig. 9 – Elemental mapping of 20-NiHCl composite (a) just after milling preparation and (b) after 2 cycles at low temperature

In Fig. 10 are presented the XRD analyses performed for 20-NiHCl composite after 2 cycles at low temperature under different hydrogenation conditions (hydrogenated, partially dehydrogenated and entirely dehydrogenated). The results obtained for fresh-milled 20-NiHCl and 20-NiHCl after 3 PCT at 300, 325 and 350 °C are shown in Fig. S10. No Mg_2NiH_4 or other Mg-Ni-H species are detected [28] but two different MgH_2 phases (tetragonal and orthorombic) are visible for the hydrogenated and partially dehydrogenated composite after cycling. They are also visible for 20-NiHCl after 3 PCT but not for the fresh-milled composite, where only tetragonal MgH_2 is detected (Fig. S10). It is therefore likely that the metastable orthorombic MgH_2 phase appears during the dehydrogenation/hydrogenation cycles. However, being present in 20-NiHCl composite after 2 cycles at low temperature and after 3

PCT at high temperature, this phase cannot explain the change in the dehydrogenation enthalpy observed in Fig. 6.

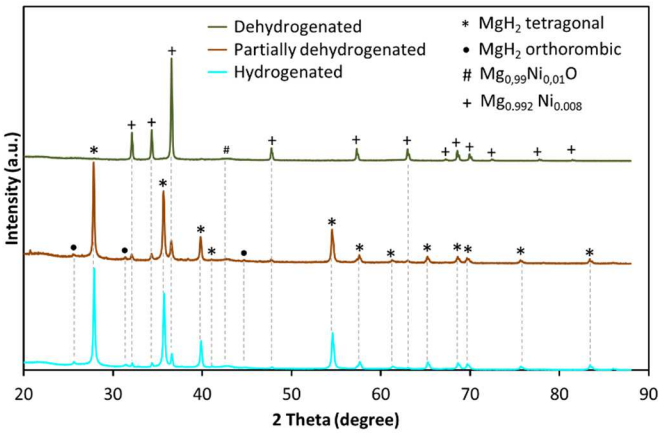

Fig. 10 – X-ray diffraction patterns of 20-NiHCl composite after two cycles at low temperature under different hydrogenation conditions

Interestingly, for all the cycled samples the XRD analyses show the presence of a $Mg_{0.992}Ni_{0.008}$ phase which is not detected for the fresh-milled composite (Fig. S10). It is therefore formed during the dehydrogenation/hydrogenation cycles. The amount of nickel detected is in good agreement with the Ni loading in 20-NiHCl composite (1.79 wt% corresponds to around 1 at%). The presence of a $Mg_{0.992}Ni_{0.008}$ phase could explain the change in the hydrogenation thermodynamics observed for 20-NiHCl composite (Fig. 8, ΔH = -65 ± 4 kJ/mol H_2 and ΔS = -120 ± 6 J/K.mol H_2). It is therefore likely that during the first dehydrogenation of 20-NiHCl composite, as the organic part of the complex decomposes, the nickel interacts with the surface of the Mg particles and forms a new metastable phase upon cycling, $Mg_{0.992}Ni_{0.008}$ with a lower hydrogenation enthalpy than the one of Mg.

Table 5 – Hydrogen storage properties of 20-NiHCl composite, comparison with data from literature

Sample	Storage capacity (wt%)	Dehydrogenation			Hydrogenation		Ref
		T_{onset} (°C)	Ea (kJ/mol)	ΔH (kJ/mol)	Ea (kJ/mol)	ΔH (kJ/mol)	
100-MgH_2	7.0	310	176	72	88	-76	This
20-NiHCl	6.3	175	127	63	22	-65	work
Ni-MHGH-75	5.4	140	64.7	62.1	22.7	-62.1	[45]
MHCH-5	< 5*	121	43	49.1	31	-46.9	[26]
MgH_2 + $Ni(C_5H_5)_2$	6.8	205	110	78	47	77	[14]
MgH_2 + $V(C_5H_5)_2$	7.0	200	80	79.6	43	-78.4	[16]
MgH_2 + $RuH_2(H_2)_2(PCy_3)_2$	6.4	279	141	83.3	/	73.6	[30]
MgH_2 + $NiCl_2(PCy_3)_2$	6.5	221	145	/	/	/	[31]
MgH_2 + Ni/CMK-3	6.0	160	43.4	74.7	37.4	/	[12]
MgH_2 + TiO_2@C	6.5	205	106	73.6	38	/	[13]

* Mg loading of only 60 %

Table 5 compares the hydrogen storage properties (thermodynamics and kinetics) of 20-NiHCl composite with results from the literature [12–14,16,26,30,31,42]. The first two systems Ni-MHGH-75 [45] and MHCH-5 [26] correspond to nanometric Mg supported on graphene and activated carbon respectively, with periodic synchronization of nickel. They present the best hydrogen storage properties with a significant increase of the kinetics and Mg/MgH_2 thermodynamics destabilization. Furthermore, the composites are stable upon cycling due to the use of carbon and graphene supports, preventing the particles aggregation at high temperature. The only limit of such systems is that the overall H_2 capacity is low in comparison with un-supported MgH_2. The remarkable hydrogen storage properties reported in these works are due to the combinative impact of the use of nanometric Mg/MgH_2 and the periodic nickel synchronization. In [26], the Mg/MgH_2 mean particles size is around 5.5 nm while it is of 5.7 nm in [45] allowing the distributed nickel to interact with both the surface and the core of the material. With a simple ball milling preparation like in 20-NiHCl composite, the mean magnesium hydride particles size is of around 250 nm as reported in previous works [30,31]. It is therefore likely that only the surface of the Mg/MgH_2 particles is doped, which can explain the difference of storage properties between the systems. Further improvement of hydrogenation and dehydrogenation kinetics and thermodynamics could therefore be achievable by using nanometric Mg/MgH_2 instead of ball milling preparation.

The other MgH_2 based composites presented in Table 5: $MgH_2 + Ni(C_5H_5)_2$ [14], $MgH_2 + V(C_5H_5)_2$ [16], $MgH_2 + RuH_2(H_2)_2(PCy_3)_2$ [30], $MgH_2 + NiCl_2PCy_3$ [31], MgH_2 + Ni/CMK-3 [12] and $MgH_2 + TiO_2$@C [13] are all using a ball-milling preparation method. Interestingly, the obtained hydrogen storage properties are in the same range but for significantly different amounts of additive present in the formed systems. For example, Chen et al. [12] used 10 wt% of Ni/CMK-3 to obtain an onset dehydrogenation temperature as low as 160 °C. Zhang et al. [13] formed a system with also 10 wt% of TiO_2@C. In 20-NiHCl, the use of only 1.79 wt% of the nickel active species allows the enhanced Mg/MgH_2 hydrogen storage properties at similar level. It is highlighting the major benefit of using transition metal complex precursors to disperse the active species at the Mg/MgH_2 particles surface instead of supported nickel or metal oxide nanoparticles.

Except for the works of Shinde et al. [26] and Xia et al. [45], only 20-NiHCl composite presents an impact on the thermodynamic stability of Mg/MgH_2. The other reported systems [12–14,16,30,31] enhance only the hydrogenation and dehydrogenation kinetics. Most of the time, the calculated H_2 release apparent activation energies are lower in the systems reported in the literature than in 20-NiHCl (80 kj/mol H_2 in [16], 106 kJ/mol H_2 in [13]… Table 5). It is likely to be due to the presence of chlorine in low amount in the complex (Fig. S8c), reported as a kinetic inhibitor for MgH_2 decomposition [31,41–43]. However, the onset dehydrogenation temperature remains in the same order of magnitude thanks to the thermodynamics destabilization observed for 20-NiHCl only. Enhancing the dehydrogenation

kinetics by substituting chlorine with other elements/groups, can be of particular interest to improve the hydrogen storage properties of Mg/MgH_2 –based storage systems.

4. Conclusion

The impact of the nickel hydride complex $NiHCl(PCy_3)_2$ on the hydrogen storage properties of the Mg/MgH_2 system has been investigated. It was observed that the complex acts as a precursor, allowing during milling preparation to homogeneously disperse nickel active species at the surface of the MgH_2 particles at an atomic or cluster scale. The composite with 20 wt% of complex presents the best storage properties. After decomposition of the organic part of the complex during the first dehydrogenation, the sample is stable upon cycling at low temperature thanks to the balance obtained between the amount of nickel involved and the site density of the catalyst over the Mg/MgH_2 particles surface. The system is able to store 6.3 wt% of H_2 at 100 °C in less than one hour and dehydrogenates at a temperature as low as 200 °C under vacuum. In comparison with the results obtained in our previous studies, 20-NiHCl composite is the first transition metal complex based system that preserves interesting hydrogenation and dehydrogenation properties after cycling.

The significantly improved hydrogen storage properties of 20-NiHCl composite in comparison with pure milled MgH_2 are due to a positive impact of highly dispersed nickel on the kinetics and thermodynamics of the Mg/MgH_2 system, thanks to the formation of a new $Mg_{0.992}Ni_{0.008}$ phase during cycling. For the dehydrogenation process, the enthalpy value was calculated to be of 63 ± 3 kJ/mol H_2 and the apparent activation energy of 127 ± 10 kJ/mol H_2. Concerning the hydrogenation of the composite, the apparent activation energy was found to be as low as 22 ± 6 kJ/mol H_2 and the enthalpy of -65 ± 4 kJ/mol H_2.

The results obtained in this study show that mixing a nickel hydride complex with MgH_2 offers promising perspectives. It is likely that further enhancement of the hydrogen storage properties could be achievable by reducing the size of the Mg/MgH_2 particles or by modifying the organometallic precursor while preserving the high availability of the dispersed nickel active species to interact with Mg/MgH_2.

Conflicts of interest

There are no conflicts to declare.

Acknowledgements

This work was supported by the French National Research Agency (Agence Nationale de la Recherche, Projet ANR-15-CE29-0023-01). The authors are thankful for the scientific services of IRCELYON, particularly Y. Aizac for XRD analyses, C. Lorentz for NMR analyses, L. Cardenaz for XPS analyses and M. Aouine for TEM analyses. They also thank CNRS for support and Dr Yannick Coppel at LCC for solid state NMR measurements.

References

[1] Abe JO, Popoola API, Ajenifuja E, Popoola OM. Hydrogen energy, economy and storage: Review and recommendation. Int J Hydrogen Energy 2019;44:15072–86. doi:10.1016/j.ijhydene.2019.04.068.

[2] Sadhasivam T, Kim H-T, Jung S, Roh S-H, Park J-H, Jung H-Y. Dimensional effects of nanostructured Mg/MgH_2 for hydrogen storage applications: A review. Renewable and Sustainable Energy Reviews 2017;72:523–34. doi:10.1016/j.rser.2017.01.107.

[3] Jain IP, Lal C, Jain A. Hydrogen storage in Mg: A most promising material. Int J Hydrogen Energy 2010;35:5133–44. doi:10.1016/j.ijhydene.2009.08.088.

[4] Klebanoff LE, Keller JO. 5 Years of hydrogen storage research in the U.S. DOE Metal Hydride Center of Excellence (MHCoE). Int J Hydrogen Energy 2013;38:4533–76. doi:10.1016/j.ijhydene.2013.01.051.

[5] DOE Technical Targets for Onboard Hydrogen Storage for Light-Duty Vehicles | Department of Energy n.d. https://www.energy.gov/eere/fuelcells/doe-technical-targets-onboard-hydrogen-storage-light-duty-vehicles (accessed October 25, 2018).

[6] Bérubé V, Radtke G, Dresselhaus M, Chen G. Size effects on the hydrogen storage properties of nanostructured metal hydrides: A review. Int J Energy Res 2007;31:637–63. doi:10.1002/er.1284.

[7] Yartys VA, Lototskyy MV, Akiba E, Albert R, Antonov VE, Ares JR, et al. Magnesium based materials for hydrogen based energy storage: Past, present and future. Int J Hydrogen Energy 2019;44:7809–59. doi:10.1016/j.ijhydene.2018.12.212.

[8] Zhang J, Zhu Y, Yao L, Xu C, Liu Y, Li L. State of the art multi-strategy improvement of Mg-based hydrides for hydrogen storage. J Alloys Compd 2019;782:796–823. doi:10.1016/j.jallcom.2018.12.217.

[9] Callini E, Aguey-Zinsou K-F, Ahuja R, Ares JR, Bals S, Biliškov N, et al. Nanostructured materials for solid-state hydrogen storage: A review of the achievement of COST Action MP1103. Int J Hydrogen Energy 2016;41:14404–28. doi:10.1016/j.ijhydene.2016.04.025.

[10] Xu X, Song C. Improving hydrogen storage/release properties of magnesium with nano-sized metal catalysts as measured by tapered element oscillating microbalance. Applied Catalysis A: General 2006;300:130–8. doi:10.1016/j.apcata.2005.10.062.

[11] Chen B-H, Chuang Y-S, Chen C-K. Improving the hydrogenation properties of MgH_2 at room temperature by doping with nano-size ZrO_2 catalyst. J Alloys Compd 2016;655:21–7. doi:10.1016/j.jallcom.2015.09.163.

[12] Chen G, Zhang Y, Chen J, Guo X, Zhu Y, Li L. Enhancing hydrogen storage performances of MgH_2 by Ni nano-particles over mesoporous carbon CMK-3. Nanotechnology 2018;29:265705. doi:10.1088/1361-6528/aabcf3.

[13] Zhang X, Leng Z, Gao M, Hu J, Du F, Yao J, et al. Enhanced hydrogen storage properties of MgH_2 catalyzed with carbon-supported nanocrystalline TiO_2. Journal of Power Sources 2018;398:183–92. doi:10.1016/j.jpowsour.2018.07.072.

[14] Kumar S, Jain A, Miyaoka H, Ichikawa T, Kojima Y. Catalytic effect of bis (cyclopentadienyl) nickel II on the improvement of the hydrogenation-dehydrogenation of Mg-MgH_2 system. Int J Hydrogen Energy 2017;42:17178–83. doi:10.1016/j.ijhydene.2017.05.090.

[15] Cheng H, Chen G, Zhang Y, Zhu Y, Li L. Boosting low-temperature de/re-hydrogenation performances of MgH_2 with Pd-Ni bimetallic nanoparticles supported by mesoporous carbon. Int J Hydrogen Energy 2019;44:10777–87. doi:10.1016/j.ijhydene.2019.02.218.

[16] Kumar S, Kojima Y, Kain V. XPS study on the vanadocene-magnesium system to understand the hydrogen sorption reaction mechanism under room temperature. Int J Hydrogen Energy 2019;44:2981–7. doi:10.1016/j.ijhydene.2018.12.053.
[17] Aguey-Zinsou K-F, Ares-Fernández J-R. Hydrogen in magnesium: new perspectives toward functional stores. Energy Environ Sci 2010;3:526–43. doi:10.1039/B921645F.
[18] Bohmhammel K, Wolf U, Wolf G, Königsberger E. Thermodynamic optimization of the system magnesium–hydrogen. Thermochimica Acta 1999;337:195–9. doi:10.1016/S0040-6031(99)00235-X.
[19] Bogdanović B, Bohmhammel K, Christ B, Reiser A, Schlichte K, Vehlen R, et al. Thermodynamic investigation of the magnesium–hydrogen system. J Alloys Compd 1999;282:84–92. doi:10.1016/S0925-8388(98)00829-9.
[20] Li J, Li B, Shao H, Li W, Lin H. Catalysis and Downsizing in Mg-Based Hydrogen Storage Materials. Catalysts 2018;8:89. doi:10.3390/catal8020089.
[21] Kumar S, Singh A, Tiwari GP, Kojima Y, Kain V. Thermodynamics and kinetics of nano-engineered Mg-MgH_2 system for reversible hydrogen storage application. Thermochimica Acta 2017;652:103–8. doi:10.1016/j.tca.2017.03.021.
[22] Zhang T, Isobe S, Jain A, Wang Y, Yamaguchi S, Miyaoka H, et al. Enhancement of hydrogen desorption kinetics in magnesium hydride by doping with lithium metatitanate. J Alloys Compd 2017;711:400–5. doi:10.1016/j.jallcom.2017.03.361.
[23] Chen M, Xiao X, Zhang M, Zheng J, Liu M, Wang X, et al. Highly dispersed metal nanoparticles on TiO_2 acted as nano redox reactor and its synergistic catalysis on the hydrogen storage properties of magnesium hydride. Int J Hydrogen Energy 2019;44:15100–9. doi:10.1016/j.ijhydene.2019.04.047.
[24] Ismail M, Mustafa NS, Ali NA, Sazelee NA, Yahya MS. The hydrogen storage properties and catalytic mechanism of the $CuFe_2O_4$-doped MgH_2 composite system. Int J Hydrogen Energy 2019;44:318–24. doi:10.1016/j.ijhydene.2018.04.191.
[25] Sazelee NA, Idris NH, Md Din MF, Mustafa NS, Ali NA, Yahya MS, et al. Synthesis of $BaFe_{12}O_{19}$ by solid state method and its effect on hydrogen storage properties of MgH_2. Int J Hydrogen Energy 2018;43:20853–60. doi:10.1016/j.ijhydene.2018.09.125.
[26] Shinde SS, Kim D-H, Yu J-Y, Lee J-H. Self-assembled air-stable magnesium hydride embedded in 3-D activated carbon for reversible hydrogen storage. Nanoscale 2017;9:7094–103. doi:10.1039/C7NR01699A.
[27] Ali NA, Idris NH, Md Din MF, Yahya MS, Ismail M. Nanoflakes $MgNiO_2$ synthesised via a simple hydrothermal method and its catalytic roles on the hydrogen sorption performance of MgH_2. J Alloys Compd 2019;796:279–86. doi:10.1016/j.jallcom.2019.05.048.
[28] Dai JH, Song Y, Yang R. First Principles Study on Hydrogen Desorption from a Metal (=Al, Ti, Mn, Ni) Doped MgH_2 (110) Surface. J Phys Chem C 2010;114:11328–34. doi:10.1021/jp103066g.
[29] Yang WN, Shang CX, Guo ZX. Site density effect of Ni particles on hydrogen desorption of MgH_2. Int J Hydrogen Energy 2010;35:4534–42. doi:10.1016/j.ijhydene.2010.02.047.
[30] Galey B, Auroux A, Sabo-Etienne S, Grellier M, Dhaher S, Postole G. Impact of the addition of poly-dihydrogen ruthenium precursor complexes on the hydrogen storage properties of the Mg/MgH_2 system. Sustainable Energy Fuels 2018;2:2335–44. doi:10.1039/C8SE00170G.
[31] Galey B, Auroux A, Sabo-Etienne S, Grellier M, Postole G. Enhancing hydrogen storage properties of the Mg/MgH_2 system by the addition of

bis(tricyclohexylphosphine)nickel(II) dichloride. Int J Hydrogen Energy 2019;44:11939–52. doi:10.1016/j.ijhydene.2019.03.114.
[32] Green MLH, Saito T, Tanfield PJ. Stable nickel hydride complexes of tricyclohexylphosphine and triisopropylphosphine. J Chem Soc A 1971:152–4. doi:10.1039/J19710000152.
[33] Green MLH, Saito T. A stable nickel hydride complex: trans-hydridochlorobis(tricyclohexylphosphine)nickel. J Chem Soc D 1969:208b–208. doi:10.1039/C2969000208B.
[34] Green MLH, Munakata H, Saito T. Hydridoborohydridobis(tricyclohexylphosphine)nickel: a new route to the preparation of nickel and palladium hydride complexes. J Chem Soc D 1969:1287a–1287a. doi:10.1039/C2969001287A.
[35] Kissinger HE. Reaction Kinetics in Differential Thermal Analysis. Anal Chem 1957;29:1702–6. doi:10.1021/ac60131a045.
[36] Farjas J, Roura P. Exact analytical solution for the Kissinger equation: Determination of the peak temperature and general properties of thermally activated transformations. Thermochimica Acta 2014;598:51–8. doi:10.1016/j.tca.2014.10.024.
[37] Moretto P, Zlotea C, Dolci F, Amieiro A, Bobet J-L, Borgschulte A, et al. A Round Robin Test exercise on hydrogen absorption/desorption properties of a magnesium hydride based material. Int J Hydrogen Energy 2013;38:6704–17. doi:10.1016/j.ijhydene.2013.03.118.
[38] Flanagan TB, Park C-N, Oates WA. Hysteresis in solid state reactions. Progress in Solid State Chemistry 1995;23:291–363. doi:10.1016/0079-6786(95)00006-G.
[39] Fanfoni M, Tomellini M. The Johnson-Mehl- Avrami-Kohnogorov model: A brief review. Nouv Cim D 1998;20:1171–82. doi:10.1007/BF03185527.
[40] Zhang Q, Zang L, Huang Y, Gao P, Jiao L, Yuan H, et al. Improved hydrogen storage properties of MgH_2 with Ni-based compounds. Int J Hydrogen Energy 2017;42:24247–55. doi:10.1016/j.ijhydene.2017.07.220.
[41] Ismail M, Mustafa NS, Juahir N, Yap FAH. Catalytic effect of $CeCl_3$ on the hydrogen storage properties of MgH_2. Materials Chemistry and Physics 2016;170:77–82. doi:10.1016/j.matchemphys.2015.12.021.
[42] Wang J, Du Y, Sun L, Li X. Effects of F and Cl on the stability of MgH_2. Int J Hydrogen Energy 2014;39:877–83. doi:10.1016/j.ijhydene.2013.10.135.
[43] Ma L-P, Kang X-D, Dai H-B, Liang Y, Fang Z-Z, Wang P-J, et al. Superior catalytic effect of TiF_3 over $TiCl_3$ in improving the hydrogen sorption kinetics of MgH_2: Catalytic role of fluorine anion. Acta Materialia 2009;57:2250–8. doi:10.1016/j.actamat.2009.01.025.
[44] Hanada N, Ichikawa T, Fujii H. Catalytic Effect of Nanoparticle 3d-Transition Metals on Hydrogen Storage Properties in Magnesium Hydride MgH_2 Prepared by Mechanical Milling. J Phys Chem B 2005;109:7188–94. doi:10.1021/jp044576c.
[45] Xia G, Tan Y, Chen X, Sun D, Guo Z, Liu H, et al. Monodisperse Magnesium Hydride Nanoparticles Uniformly Self-Assembled on Graphene. Advanced Materials 2015;27:5981–8. doi:10.1002/adma.201502005.

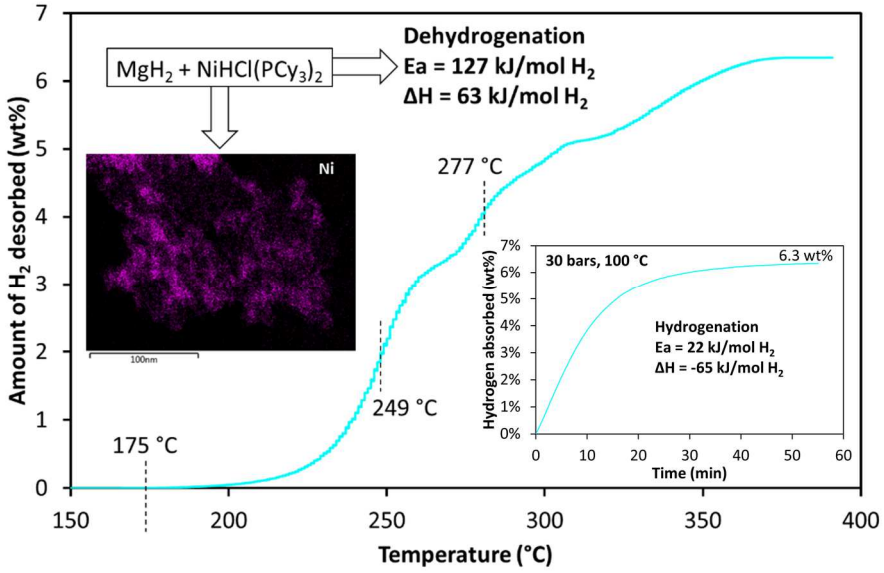
MgH2 + NiHCl(PCy3)2
Dehydrogenation
Ea = 127 kJ/mol H2
ΔH = 63 kJ/mol H2
Ni
100nm
277 °C
249 °C
175 °C
30 bars, 100 °C
6.3 wt%
Hydrogenation
Ea = 22 kJ/mol H2
ΔH = -65 kJ/mol H2
Hydrogen absorbed (wt%)
Time (min)
Amount of H2 desorbed (wt%)
Temperature (°C)